

Title	Pore formation in InP anodized in KOH: Effect of temperature and concentration
Authors	Quill, Nathan;Lynch, Robert P.;O'Dwyer, Colm;Buckley, D. Noel
Publication date	2013-07
Original Citation	Quill, N., Lynch, R. P., O'Dwyer, C. and Buckley, D. N. [2013] 'Pore Formation in InP Anodized in KOH: Effect of Temperature and Concentration', ECS Transactions, 50(37), pp. 131-141. doi: 10.1149/05037.0131ecst
Type of publication	Article (peer-reviewed)
Link to publisher's version	http://ecst.ecsdl.org/content/50/37/131.abstract - 10.1149/05037.0131ecst
Rights	© 2013 ECS - The Electrochemical Society
Download date	2024-05-14 03:56:06
Item downloaded from	https://hdl.handle.net/10468/6159

Pore Formation in InP Anodized in KOH: Effect of Temperature and Concentration

N. Quill^{1,2}, R. P. Lynch^{1,2}, C. O'Dwyer^{3,4}, D. N. Buckley^{1,2}

¹*Department of Physics and Energy, University of Limerick, Limerick Ireland*

²*Materials and Surface Science Institute, University of Limerick, Limerick Ireland*

³*Applied Nanoscience Group, Department of Chemistry, University College Cork, Cork Ireland*

⁴*Micro & Nanoelectronics Centre, Tyndall National Institute, Lee Maltings, Cork, Ireland*

The effect of both temperature and electrolyte concentration on the formation of porous layers in InP is explored. Pore width, porous layer thickness and porosity decrease with increasing temperature and show a minimum at intermediate KOH concentrations, increasing as concentration is either increased or decreased from that value. The variations in pore width and layer thickness are correlated: thinner pores appear to limit layer thickness, presumably by influencing mass transport throughout the porous network. A three step model of charge transfer at the semiconductor/electrolyte interface is used to explain these observations.

INTRODUCTION

Although the formation of porous silicon in HF has been long known,¹⁻⁴ the discovery of visible luminescence from porous silicon⁵ sparked the surge in research interest in the formation of porosity in other semiconductors. The list of semiconductors that can now be rendered porous electrochemically includes germanium,⁶⁻⁸ GaP,⁹⁻¹¹ InP,¹²⁻¹⁸ GaAs,¹⁹⁻²³ GaN,²⁴⁻²⁶ and many others. A range of different pore morphologies can be obtained in these semiconductors by variation of electrolyte type and concentration,^{14,27} carrier concentration and substrate orientation,^{28,29} as well as the current density or potential used to form the porous structure.³⁰ A number of theories have been proposed^{2-4,31-34} to explain the plethora of pore morphologies that have been observed with various semiconductor/electrolyte combinations but, so far, no one theory has been able to explain all observations.

In our group, we have demonstrated the formation of porous InP in KOH electrolytes in the concentration range 1-10 mol dm⁻³.^{18,35} We have previously shown that pores emerge from pits in the electrode surface³⁶ and grow and branch along the <111>A crystallographic directions, forming tetrahedral porous domains.³⁷ In this paper, InP is anodized in KOH concentrations ranging from 2.5 to 17 mol dm⁻³. The effect of temperature on porous InP formation will also be explored.

EXPERIMENTAL

The working electrode consisted of polished (100)-oriented monocrystalline sulphur doped ($n = 5 - 5.6 \times 10^{18} \text{ cm}^{-3}$) n-InP. An ohmic contact was made to the back of the InP

electrode and the back and sides of the electrode were isolated electrically from the electrolyte by means of a suitable varnish. The electrode area was typically 0.2 cm^2 . The etch pit density of all samples used was less than $5 \times 10^3 \text{ cm}^{-2}$. Anodisation was carried out in aqueous KOH electrolytes at a range of concentrations and temperatures. A conventional three-electrode cell configuration was used employing a platinum counter electrode and a saturated calomel reference electrode (SCE) to which all potentials were referenced. Prior to immersion in the electrolyte, the working electrode was dipped in an etchant (3:1:1 $\text{H}_2\text{SO}_4\text{:H}_2\text{O}_2\text{:H}_2\text{O}$) for 4 minutes and then rinsed in deionised water. All electrochemical experiments were carried out in the absence of light. The temperature was held constant by a thermostatic water bath connected to a water jacket cell in which the experiments were carried out.

A CH Instruments Model 650A Electrochemical Workstation was employed for cell parameter control and for data acquisition. Cleaved {011} cross-sections and the (100) surfaces were examined using a Hitachi S-4800 field-emission scanning electron microscope (SEM) operating at 5 kV.

RESULTS AND DISCUSSION

The Effect of Temperature on Porous Layer Formation

Anodisation of n-InP samples by linear potential sweep (LPS) was carried out at a range of temperatures in 9 mol dm^{-3} KOH at a scan rate of 2.5 mV s^{-1} . At 10°C the linear sweep voltammogram (LSV) exhibits two current peaks, which will be referred to as P_1 (the peak which occurs at the lower potential) and P_2 (the peak which occurs at the higher potential) hereafter. As the LPSs are performed at increasingly high temperatures, these two peaks occur closer together until eventually, at 40°C and above, only a single peak is observed.

SEM micrographs of InP electrodes which have undergone linear potential sweeps at various temperatures are shown in Fig. 2. Typical $\langle 111 \rangle$ aligned pore growth³⁷ is seen on all samples. A plot of porous layer thickness against anodisation temperature as measured from SEM micrographs of the (011) cross section is shown in Fig. 3. The porous layer thickness decreases as the temperature is increased. The trend of decreasing layer thickness with increasing temperature explains the shift from double peak to single peak in the LSVs in Fig. 1. As previously reported,²⁸ P_1 is associated with the merging of individual porous domains to form a continuous porous layer. For shallower porous layers, the merging of domains either coincides with, or occurs after, the beginning of the decay in current due to the cessation of porous layer etching. As a result, samples with shallower layers exhibit only one current peak.

The variation of pore width with anodisation temperature is also shown in Fig. 3. The average pore width decreases as the temperature is increased. The variation of pore width with temperature shows a very similar trend to that of layer thickness. This is shown more clearly in the inset of Fig. 3 which is a plot of layer thickness against pore width. This correlation indicates that whatever is responsible for the cessation of porous layer growth may also be related to the characteristic value of pore width. Significant oxide deposits are often observed within the pores of fully grown layers. It may be that the thinner pores are more susceptible to clogging by oxide precipitates and this causes growth for these pores to cease more quickly.

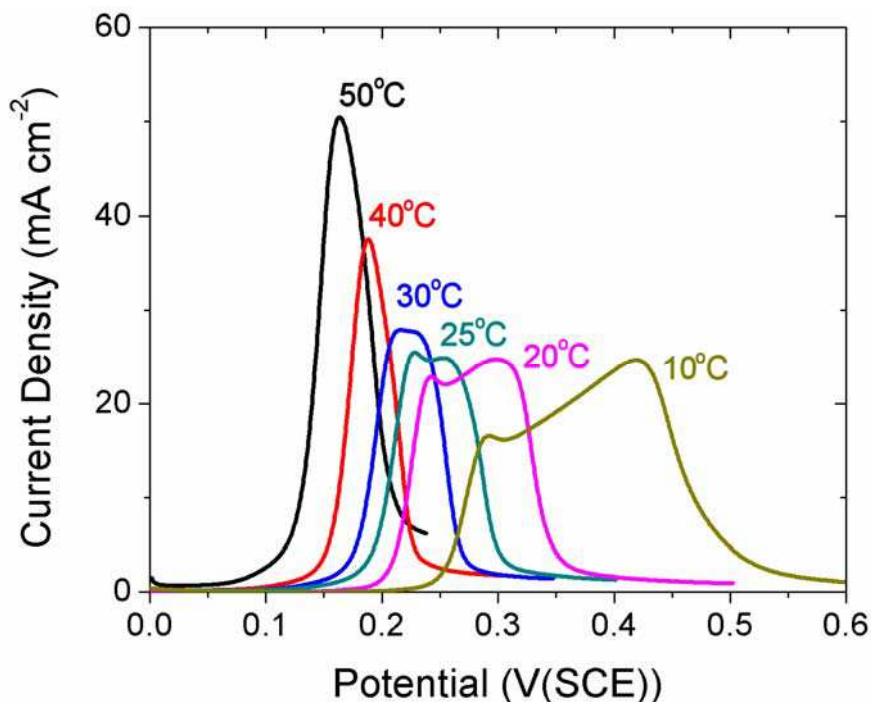


Figure 1. LSVs of InP in 9 mol dm⁻³ KOH at varying temperatures. The temperature of anodisation varies from 50°C to 10°C from left to right.

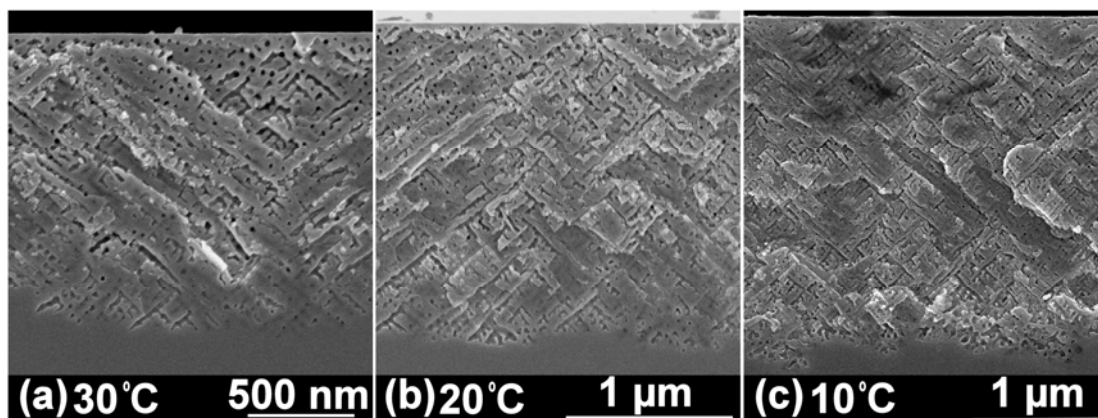


Figure 2. Cross-sectional SEM micrographs of the (011) plane of InP electrodes after anodisation in 9 mol dm⁻³ KOH as in Fig. 1. The temperature at which each porous layer was formed was (a) 30°C, (b) 20°C and (c) 10°C.

A plot of the porosity of a porous layer (calculated by comparing the expected etch depth for planar etching of InP from Faraday's law to the porous layer thickness) against temperature is shown in Fig. 4. The porosity can be seen to generally decrease with increasing temperature in a similar manner to both pore width and layer thickness. The variation in porosity indicates that when the pore width decreased, the pore wall thickness did not decrease in proportion as temperature was varied; i.e. pore diameter decreased significantly with increasing temperature but pore wall thickness did not decrease as significantly over the same temperature range. It is generally accepted that the region at the pore tip where etching can occur (and therefore the diameter of the pores) is set by a characteristic length scale which is determined by the depletion layer

width of the material and the electric field at the pore tip⁴. Similarly, the thickness of the inter pore spacing (*i.e.* the pore walls) is determined by the depletion layer thickness². The electric field at a pore tip is determined by the curvature of the pore tip⁴. Therefore, if there is no change in tip curvature, both the pore wall thickness and the pore diameter should be determined by the same characteristic length scale (*i.e.* the depletion layer width of the material). It follows that a change in pore width would be expected to be accompanied by a change in pore wall thickness, and little change in porosity should be observed. It is likely then that the characteristic length scale did not change and the increased pore width is a result of pore walls being etched to a greater extent at lower temperatures.

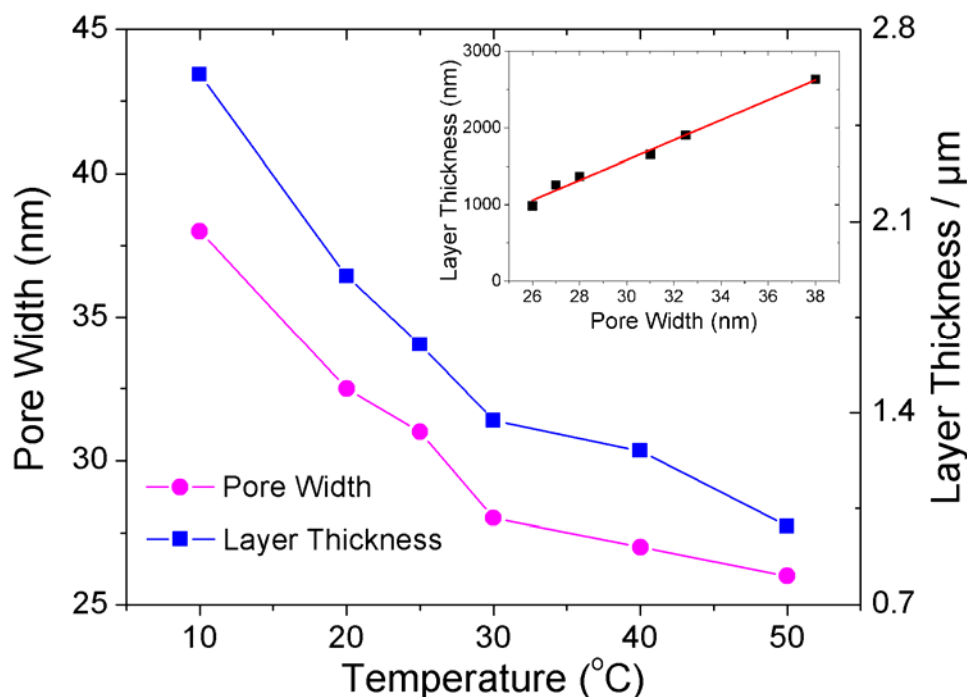


Figure 3. Plot of both pore width and porous layer thickness against temperature for InP electrodes subjected to LPSs at different temperatures in 9 mol dm⁻³ KOH as in Fig. 1. The inset is a plot of pore width against layer thickness, with the linear trend-line highlighting the correlation between the two quantities as temperature is varied.

The Effect of KOH Concentration on Porous Layer Formation

The formation of porous InP in KOH concentrations ranging from 2 to 10 mol dm⁻³ has been reported previously.^{18,35} Figure 5 shows LSVs of InP samples anodized in KOH concentrations ranging from 2.5 to 17 mol dm⁻³ KOH. Both the current density at P₂ and the potential at P₁ decrease with increasing KOH concentration. For the samples anodized in 9 mol dm⁻³ or lower, the separation between P₁ and P₂ decreases as the concentration is increased. Above 9 mol dm⁻³ however, the separation between the peaks increases again.

SEM micrographs of some porous layers grown at different concentrations are shown in Fig. 6. All samples exhibited typical <111>_A oriented pore growth. As with the variation of temperature, the variation of KOH concentration also affected both the pore width and the porous layer thickness. The variation in both of these porous layer properties is plotted in Fig. 7 and it can be seen that again, the pore width and the layer

thickness are correlated. Both pore width and layer thickness show a minimum at 9 mol dm⁻³ KOH and increase as the concentration is either increased or decreased from this value.

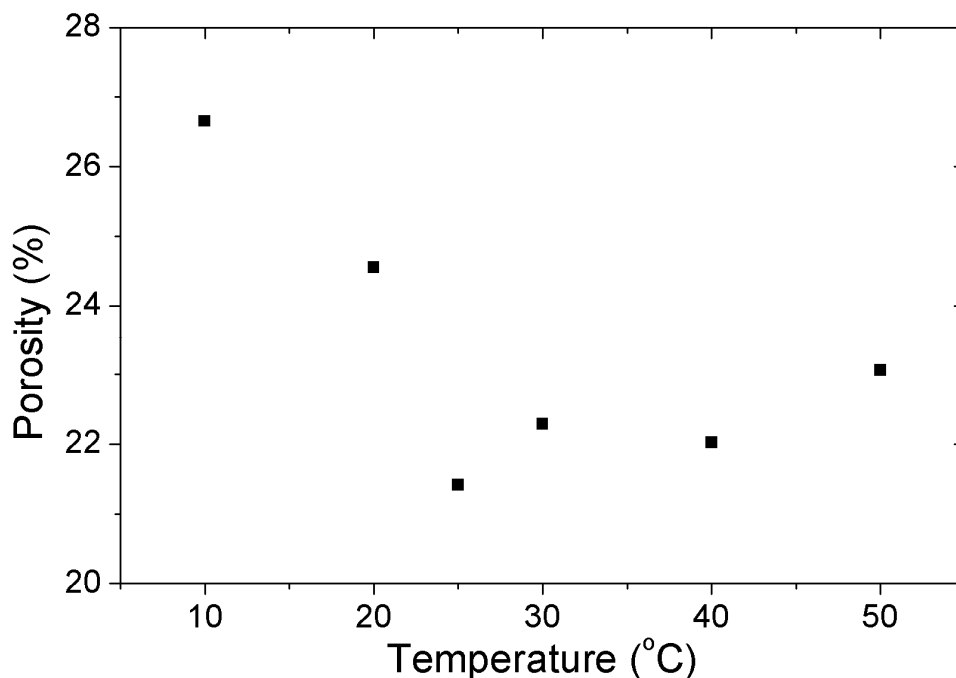


Figure 4. Plot of percentage porosity against temperature for the samples anodized at different temperatures as in Fig. 1.

The increase in separation between P_1 and P_2 seen for concentrations above 9 mol dm⁻³ can be explained by the increase in layer thickness above this concentration. As previously mentioned P_1 is associated with discrete porous domains merging to form a complete porous layer across the entire electrode surface.²⁸ The second peak occurs due to the cessation of porous layer growth. The separation between the peaks is therefore indicative of how long the porous layer continued growing after domain merging had occurred. Thus, the greater layer thicknesses seen above 9 mol dm⁻³ led to a greater separation between P_1 and P_2 .

Both porous layer thickness and pore width decrease with increasing concentration between 2.5 mol dm⁻³ and 9 mol dm⁻³. Similar trends have been observed previously for InP in KOH^{18,35} and for Si anodized in HF.³⁸ However above 9 mol dm⁻³, Fig. 7 shows the opposite trend: both pore width and layer thickness increase with increasing concentration.

Figure 8 shows the variation of porosity with KOH concentration. The porosity decreases with increasing KOH concentration initially, but begins to increase again as the KOH concentration is increased further. This is the same trend that was seen for layer thickness and pore width in Fig. 7. The fact that porosity increases as the pore width increases, at concentrations above 9 mol dm⁻³, indicates that the increase in pore width is not being compensated for by a proportional increase in the pore wall thickness *i.e.* the pore width increase is due to the increased etching of pore walls and not due to a change in the characteristic length scale of the pore structure.

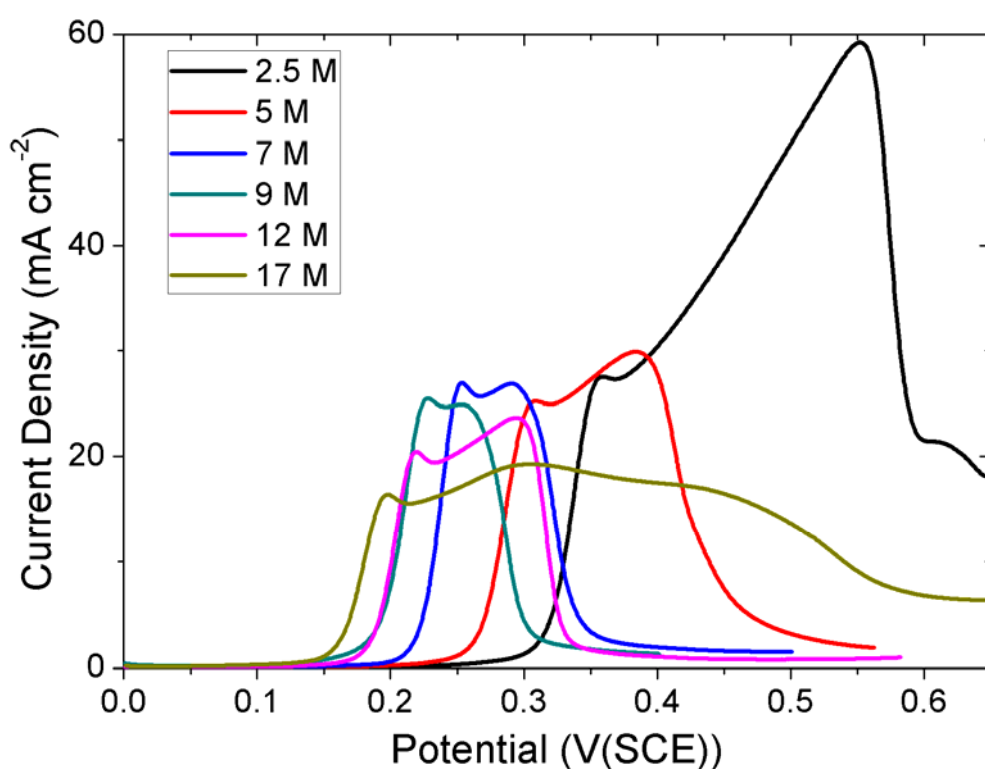


Figure 5. LSVs of InP electrodes anodized in a range of KOH concentrations at 2.5 mV s^{-1} at 25°C . The concentration was varied from 2.5 mol dm^{-3} to 17 mol dm^{-3} .

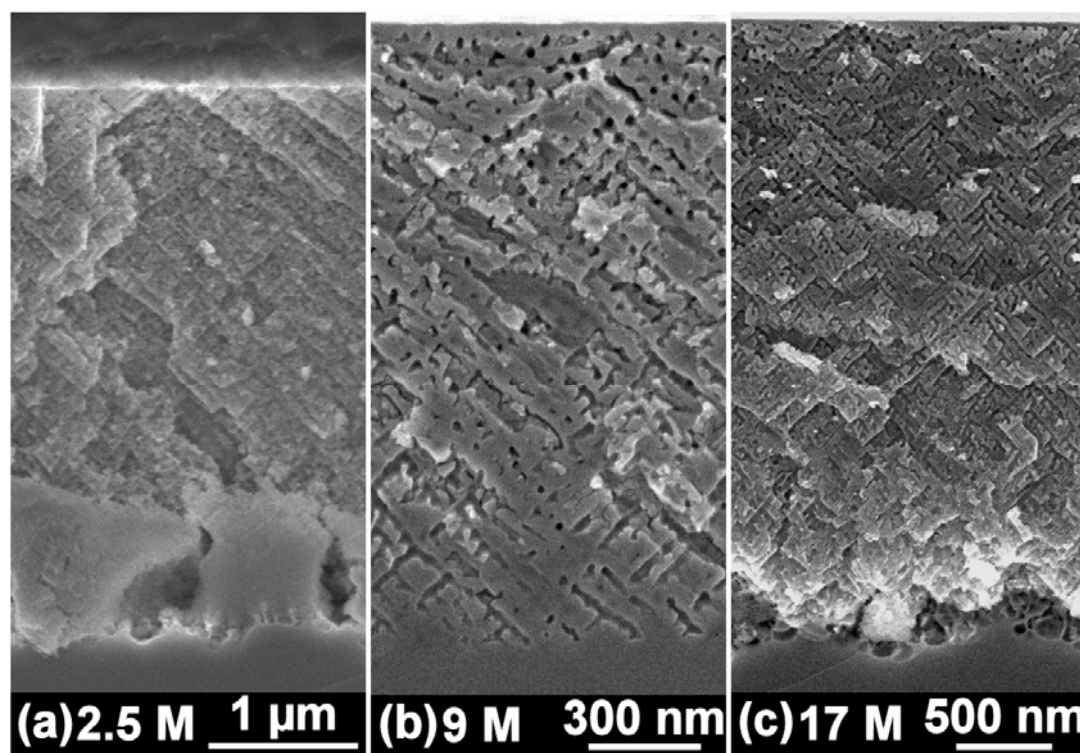


Figure 6. A series of SEM micrographs of InP electrodes anodized in a range of KOH concentrations at 25°C . The concentration was varied from 2.5 mol dm^{-3} to 17 mol dm^{-3} .

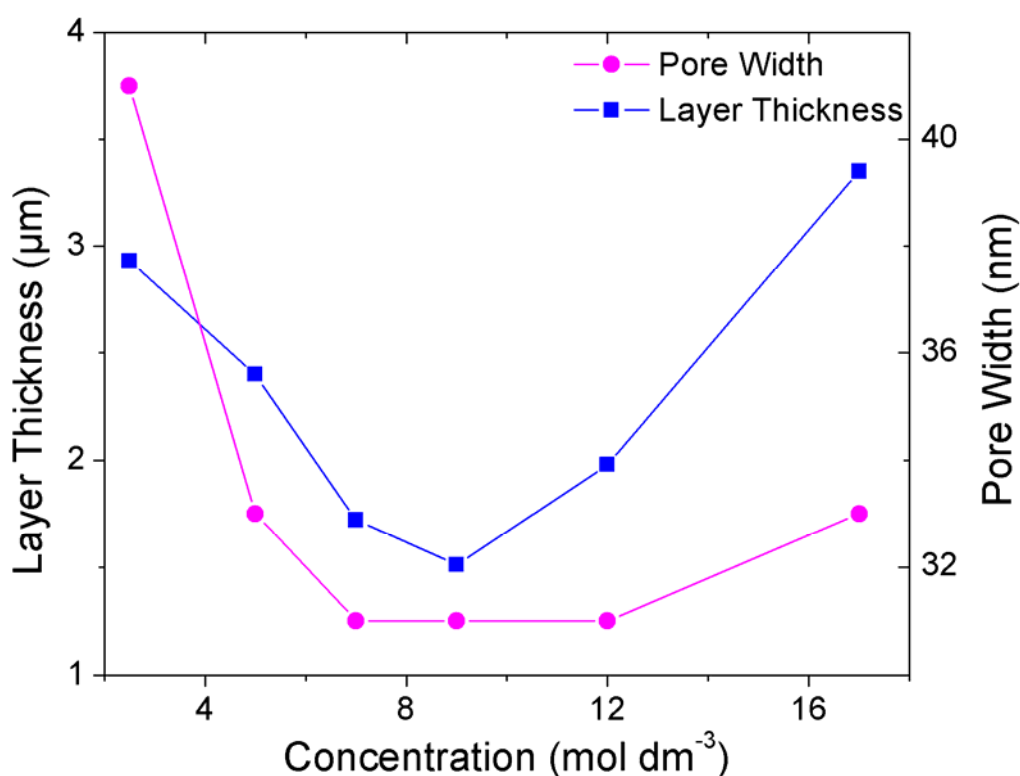


Figure 7. Plot of layer thickness (-■-) and pore width (-●-) against KOH concentration for samples anodised by LPS at 2.5 mV s^{-1} at 25°C in different concentrations of KOH (as shown in Fig. 5).

Origin of Pore Width Variation with Temperature and Concentration

Pore width variation with both temperature and concentration can be explained by consideration of a qualitative model of charge transfer between the semiconductor and the electrolyte. The basic features of the model are depicted in Fig. 9. In this model, the variation in pore width with both temperature and concentration is due to the varying rate of the electrochemical reaction at the pore tips at higher temperatures.^{39,40} Assuming that holes are supplied preferentially to a region of high curvature at a pore tip due to the enhanced electric field in that region,⁴ then there is a characteristic diameter for this pore tip; *i.e.* there exists a characteristic region at the pore tip where carriers can transfer across the depletion layer and etching can take place.^{2,4} If holes which arrive at the pore tip are instantly annihilated in an electrochemical reaction, this characteristic pore diameter would be observed. However if the holes have some time to diffuse laterally at the electrode-electrolyte interface before being removed electrochemically, the result would be less spatially confined etching *i.e.* wider pores. The measured value of pore width would then be dictated by a combination of the electric field distribution at the pore tip and the kinetics of the electrochemical reaction. At higher temperatures, the rate of the electrochemical reaction is expected to be higher and so the amount of time a hole has to diffuse at the interface is shorter. Consequently, the effective diffusion length is shorter, leading to more spatially confined etching. This effect may lead to the asymptotic approach to the characteristic pore diameter (defined by the electric field distribution) that is observed as temperature is increased.

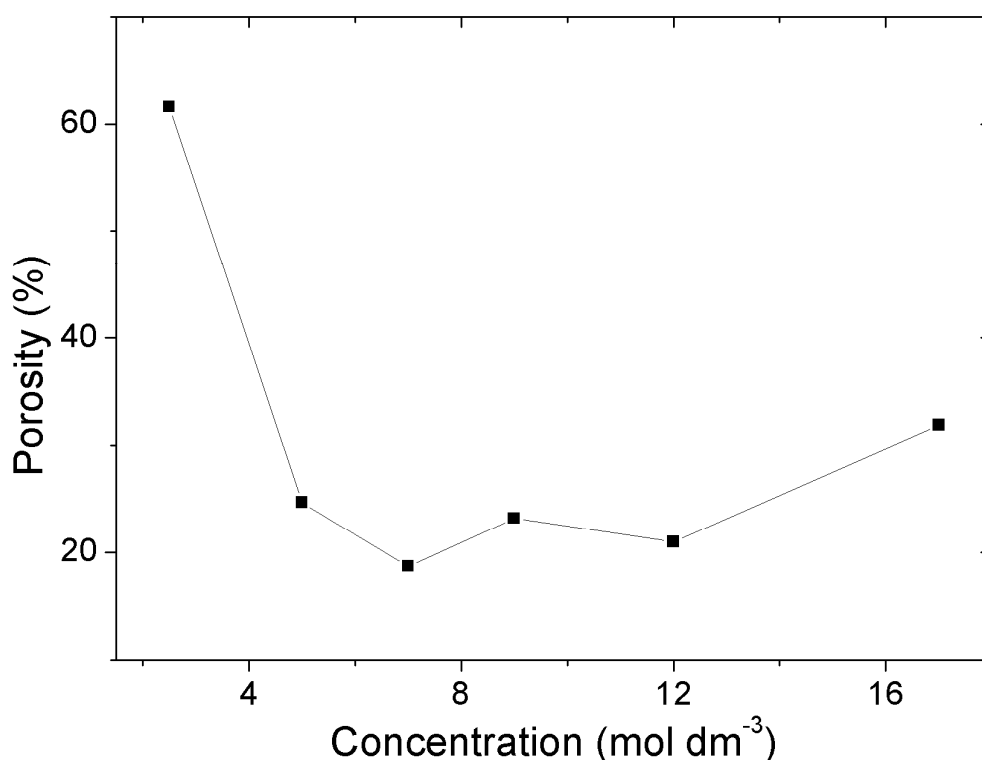


Figure 8. Plot of percentage porosity against KOH concentration for samples anodized by LPS at 2.5 mV s^{-1} at 25°C in different concentrations of KOH (as shown in Fig. 5).

The increase in porosity that was observed as temperature was decreased (see Fig. 4) is also consistent with this model. It was noted earlier that an increase in porosity accompanied by an increase in pore width indicates that this pore width increase is facilitated by further etching of the pore walls and not by a change in the characteristic length scale (depletion layer width) of the porous structure. This supports the idea that it is the increased effective diffusion length of holes at the pore tip which leads to wider pores at lower temperatures.

The decrease in pore width as KOH concentration is increased in the range of $2.5 - 9 \text{ mol dm}^{-3}$ can be explained by the same model used to explain the variation of pore width with temperature. As the electrolyte concentration is increased, holes which tunnel through the depletion layer at the pore tip may have less time to diffuse laterally at the interface before being removed electrochemically. This is attributed to an increase in the rate of reaction (rate of consumption of holes) as the concentration of KOH is increased. Thus, at higher KOH concentrations, etching is spatially confined and the average pore width decreases.

Above 9 mol dm^{-3} the pore width increases again. This increase suggests that the rate of the electrochemical reaction decreases above this concentration. Interestingly, reported values for the specific conductivity of KOH show that it reaches a maximum at approximately 7 mol dm^{-3} and decreases with increasing concentration after that.⁴¹ This suggests that a change in the structure of the electrolyte occurs at higher concentrations which may result in a decrease in the kinetics of the relevant electrochemical reaction as expected from the mechanism we have presented here. The variation in porosity with concentration, which was correlated with the changes in pore width, supports the idea

that it is the increased etching of pore walls which leads to the observation of wider pores, *i.e.* the increased effective diffusion length of holes at the pore tip results in less spatially confined etching, such that the pore width increases without a change in the characteristic length scale of the pore structure.

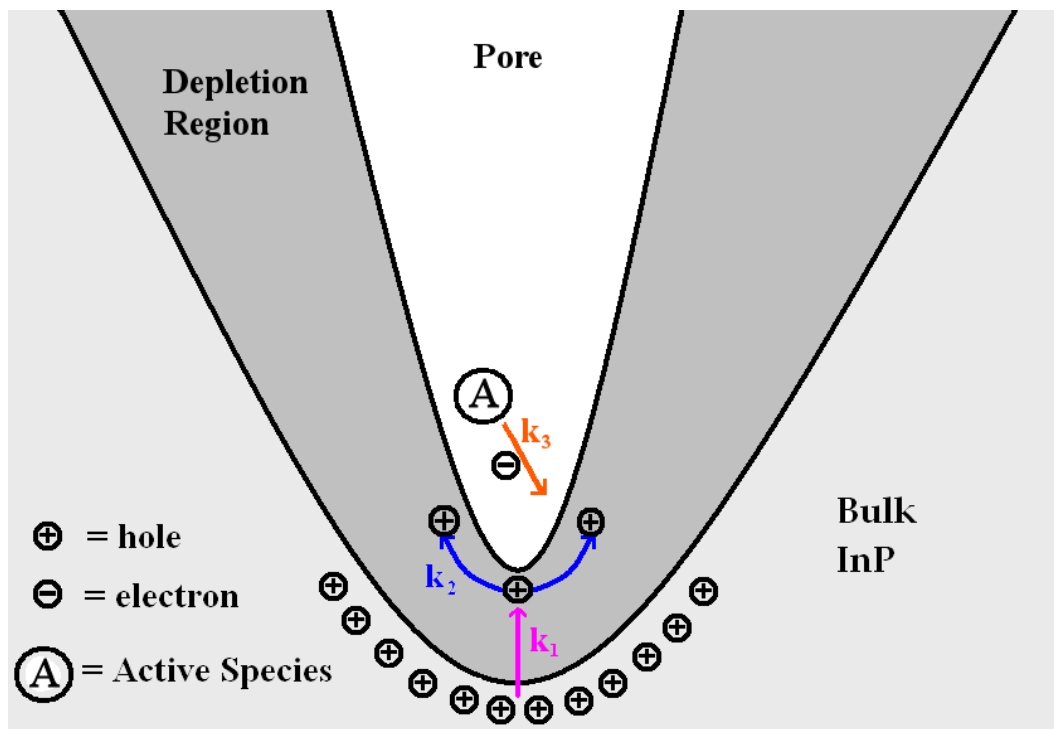


Figure 9. Schematic of the three-step charge transfer mechanism which argues that pore width is determined both by the rate of hole diffusion at the surface and the relative reactivity of the active species in solution. k_1 represents the rate at which holes are supplied to the pore tip, k_2 represents the characteristic diffusion rate of holes at the semiconductor/electrolyte interface and k_3 represents the rate at which the active species in solution captures holes from (injects electrons into) the semiconductor.

CONCLUSIONS

In experiments in which porous layers were formed at different temperatures, the pore width decreased as the temperature at which the pores were formed increased. The decrease in pore width was correlated with a decrease in layer thickness, and a decrease in the porosity. The correlation between pore width and layer thickness suggested that mass transport may be the main factor limiting porous layer thickness.

As the concentration of the electrolyte was increased, the pore width decreased initially up to 9 mol dm^{-3} , and then began to increase again above that. The change in behavior at 9 mol dm^{-3} may have been due to a change in the structure of the electrolyte at high concentrations. The variation of layer thickness was again correlated with the variation in both porosity and layer thickness.

A three-step model of charge transfer was used to explain the variation in pore width seen when temperature and concentration were varied. The model proposes that the pore width variations are a result of a variation in the rate of hole capture by the

electrochemical reaction at different temperatures and concentrations. This results in different effective diffusion lengths for holes at the electrode-electrolyte interface in the vicinity of the pore tip leading to variations in the spatial extent of the reaction and hence, variations in the pore width.

ACKNOWLEDGEMENTS

Two of the authors, R.P. Lynch and N. Quill, would like to thank the Irish Research Council for Science Engineering and Technology for postgraduate scholarships to perform this research.

REFERENCES

1. A. Uhler, *Bell System Technical Journal*, **35**, 333 (1956).
2. M. I. J. Beale, J. D. Benjamin, M. J. Uren, N. G. Chew and A. G. Cullis, *Journal of Crystal Growth*, **73**, 622 (1985).
3. R. L. Smith and S. D. Collins, *Journal of Applied Physics*, **71**, R1 (1992).
4. X. G. Zhang, *Journal of The Electrochemical Society*, **151**, C69 (2004).
5. L. T. Canham, *Applied Physics Letters*, **57**, 1046 (1990).
6. S. Miyazawa, K. Sakamoto, K. Shiba and M. Hirose, *Thin Solid Films*, **255**, 99 (1995).
7. M. Sendova-Vassileva, N. Tzenov, D. Dimova-Malinovska, M. Rosenbauer, M. Stutzmann and K. V. Josepovits, *Thin Solid Films*, **255**, 282 (1995).
8. S. Bayliss, Q. Zhang and P. Harris, *Appl. Surf. Sci.*, **102**, 390 (1996).
9. B. H. Erne, D. Vanmaekelbergh and J. J. Kelly, *Journal of The Electrochemical Society*, **143**, 305 (1996).
10. P. Schmuki, D. J. Lockwood, H. J. Labbe and J. W. Fraser, *Applied Physics Letters*, **69**, 1620 (1996).
11. J. Wloka, K. Mueller and P. Schmuki, *Electrochemical and Solid-State Letters*, **8**, B72 (2005).
12. A. Hamamatsu, C. Kaneshiro, H. Fujikura and H. Hasegawa, *Journal of Electroanalytical Chemistry*, **473**, 223 (1999).
13. T. Takizawa, S. Arai and M. Nakahara, *Japanese Journal of Applied Physics*, **33**, L643 (1994).
14. P. Schmuki, L. Santinacci, T. Djenizian and D. J. Lockwood, *physica status solidi (a)*, **182**, 51 (2000).
15. Z. Weng, A. Liu, Y. Sang, J. Zhang, Z. Hu, Y. Liu and W. Liu, *Journal of Porous Materials*, **16**, 707 (2009).
16. Z. Weng, W. Zhang, C. Wu, H. Cai, C. Li, Z. Wang, Z. Song and A. Liu, *Applied Surface Science*, **256**, 2052 (2010).
17. A. M. Goncalves, L. Santinacci, A. Eb, I. Gerard, C. Mathieu and A. Etcheberry, *Electrochemical and Solid-State Letters*, **10**, D35 (2007).
18. C. O'Dwyer, D. N. Buckley, D. Sutton and S. B. Newcomb, *Journal of The Electrochemical Society*, **153**, G1039 (2006).
19. G. Oskam, A. Natarajan, P. C. Searson and F. M. Ross, *Applied Surface Science*, **119**, 160 (1997).
20. M. M. Faktor, D. G. Fiddymment and M. R. Taylor, *Journal of The Electrochemical Society*, **122**, 1566 (1975).

21. P. Schmuki, J. Fraser, C. M. Vitus, M. J. Graham and H. S. Isaacs, *Journal of The Electrochemical Society*, **143**, 3316 (1996).
22. I. M. Tiginyanu, V. V. Ursaki, E. Monaico, E. Foca and H. Foll, *Electrochemical and Solid-State Letters*, **10**, D127 (2007).
23. A. M. Gonçalves, L. Santinacci, A. Eb, C. David, C. Mathieu, M. Herlem and A. Etcheberry, *physica status solidi (a)*, **204**, 1286 (2007).
24. D. J. Diaz, T. L. Williamson, I. Adesida and P. W. Bohn, *Journal of Vacuum Science and Technology (B)*, **20**, 2375 (2002).
25. A. P. Vajpeyi, S. Tripathy, S. J. Chua and E. A. Fitzgerald, *Physica E: Low-dimensional Systems and Nanostructures*, **28**, 141 (2005).
26. F. K. Yam, Z. Hassan, L. S. Chuah and Y. P. Ali, *Applied Surface Science*, **253**, 7429 (2007).
27. N. Quill, R. P. Lynch, C. O'Dwyer and D. N. Buckley, *ECS Trans.*, **this volume** (2012).
28. N. Quill, C. O'Dwyer, R. Lynch and D. N. Buckley, *ECS Transactions*, **19**, 295 (2009).
29. S. Ronnebeck, J. Carstensen, S. Ottow and H. Foll, *Electrochemical and Solid-State Letters*, **2**, 126 (1999).
30. S. Langa, I. M. Tiginyanu, J. Carstensen, M. Christophersen and H. Foll, *Electrochemical and Solid-State Letters*, **3**, 514 (2000).
31. T. Unagami, *Journal of The Electrochemical Society*, **127**, 476 (1980).
32. V. Lehmann and H. Foll, *Journal of The Electrochemical Society*, **137**, 653 (1990).
33. V. Lehmann, *Journal of The Electrochemical Society*, **140**, 2836 (1993).
34. J. Cartensen, M. Christophersen and H. Foll, *Material Science and Engineering B*, **69-70**, 23 (2000).
35. R. P. Lynch, C. O'Dwyer, D. N. Buckley, D. Sutton and S. Newcomb, *ECS Transactions*, **2**, 131 (2006).
36. C. O'Dwyer, D. N. Buckley, D. Sutton, M. Serantoni and S. B. Newcomb, *Journal of The Electrochemical Society*, **154**, H78 (2007).
37. R. P. Lynch, C. O'Dwyer, D. Sutton, S. B. Newcomb and D. N. Buckley, *ECS Transactions*, **6**, 355 (2007).
38. P. Jaguiro, S. La Monica, S. Lazononk and A. Ferrari, in *Proceedings of Pits and Pores: Formation, Properties and Significance for Advanced Luminescent Materials*, 358 (1997).
39. N. Quill, R. P. Lynch, C. O'Dwyer and D. N. Buckley, *ECS Trans.*, **this volume** (2012).
40. R. P. Lynch, N. Quill, C. O'Dwyer and D. N. Buckley, *ECS Transactions*, **this volume** (2012).
41. R. J. Gilliam, J. W. Graydon, D. W. Kirk and S. J. Thorpe, *International Journal of Hydrogen Energy*, **32**, 359 (2007).